Research Article

Ferroelectric, pyroelectric and piezoelectric properties of CeO_2-doped $Na_{0.5}Bi_{0.5}TiO_3$ ceramics

N. A. Halim[1] · W. H. Abd. Majid[1] · T. S. Velayutham[1]

Abstract

Lead-free sodium–bismuth titanate ($Na_{0.5}Bi_{0.5}TiO_3$, NBT) nanoceramics synthesized by sol–gel method were doped with CeO_2 by using solid-state method from 0.0 to 5.0 wt%. The effects of CeO_2-doped NBT on structure and microstructure as well as electrical properties were investigated. X-ray analysis shows that CeO_2 diffuses into the lattice of NBT to form a solid solution and form morphotropic phase boundary between rhombohedral and tetragonal phase structure in NBT during the sintering process. The electrical properties of NBT ceramics have been greatly improved by doping certain amount of CeO_2. The NBT-0.6 wt% CeO_2 shows improvement in dielectric properties at room temperature with the highest dielectric constant at 10 kHz ($\varepsilon_m' = 1276$, $\tan\delta = 0.03$ and $T_m = 370\ ^\circ C$), high remanent polarization ($P_r = 56\ \mu C\ cm^{-2}$) and low coercive field ($E_c = 53\ kV\ cm^{-1}$). Piezoelectric properties were enhanced with the doping, where the piezoelectric constant $d_{33} = 90\ pC\ N^{-1}$ and enhance in mechanical coupling factor $k_{33} = 0.44$. The results suggest that the NBT-0.6 CeO_2 ceramics can be a suitable material for sensor, actuator or memory device application.

Keywords Piezoelectric · Solid-state reactions · Morphotropic phase boundary (MPB) · Ferroelectric properties

1 Introduction

Ongoing demands to improve the piezoelectric properties and the operational range are constant driving force for the development of advanced piezoelectric. The extensive search efforts on the lead-free ceramics with the performance which is equivalent or even superior to that of $Pb(ZrTi)O_3$ (PZT)-based piezoeceramics resulted in the research on the three main families of solid solution: (K,Na) NbO_3-based, $Na_{0.5}Bi_{0.5}TiO_3$ (NBT)-based and $BaTiO_3$-based materials. Much attention was paid to sodium–bismuth titanate ($Na_{0.5}Bi_{0.5}TiO_3$)-based system because Bi^{3+} ions have the second highest polarizability (after Pb^{2+}) which caused by the 6 s^2 lone pairs contribute to the large structural distortions and extraordinary large strain, generated by field-induced phase transitions. NBT is a perovskite structure ceramic with rhomohedral symmetry at the room temperature and shows strong ferroelectric properties with high characteristic temperature, T_m (~ 320 °C) and large remanent polarization (~ 38–47 μC cm^{-2}) [1, 2].

For the majority of applications, the optimum performance of NBT is found at the boundary between tetragonal and rhombohedral phases known as the morphotropic phase boundary (MPB). For the compositions close to MPB, the piezoelectric coefficient maximizes as well as allows for ease of reorientation of domains or poling process [3, 4]. The MPB of a NBT ceramic can be further modified with additive such as metal oxides and rear earth oxides. For example, adding rare earth oxide such as La_2O_3, CeO_2, Y_2O_3 and Nd_2O_3 was reported to improve the piezoelectric properties of BNT-based ceramics [5–9]. However, the benefits of the dopant to the NBT depend greatly on the nature of the dopant oxides.

CeO_2 has been used as a dopant for lead ceramics such as PZT ceramics to improve density and piezoelectric properties, while it reduces the conductivity and dielectric loss of

✉ N. A. Halim, nurain.abhalim@yahoo.com; ✉ W. H. Abd. Majid, q3haliza@um.edu.my | [1]Low Dimensional Materials Research Centre, Department of Physics, Faculty of Science, University of Malaya, 50603 Kuala Lumpur, Malaysia.

SN Applied Sciences (2019) 1:582 | https://doi.org/10.1007/s42452-019-0593-2

Received: 26 November 2018 / Accepted: 10 May 2019 / Published online: 17 May 2019

the samples [10–12]. Moreover, CeO_2 is anticipated to reduce the coercive field of NBT. In this study, NBT was doped with various wt% of CeO_2 to investigate the effects of the CeO_2 on the microstructure, physical and the electrical (ferroelectric, pyroelectric, piezoelectric and dielectric) properties of the NBT ceramics.

2 Experimental

The NBT nano-powder was synthesized by sol–gel method where anhydrous sodium acetate (CH_3COONa, 99.95%), bismuth (III) acetate ($(CH_3COO)_3Bi$, 99.99 + %) and titanium (IV) butoxide ($Ti[O(CH_2)CH_3]_4$, 97%) were selected as raw materials. The detail of sol–gel procedure was published elsewhere [2]. The calcined NBT powder was doped with cerium (IV) oxide ($Ce(IV)O_2$, < 0.25 nm size powder, 99%, Sigma-Aldrich) with various weight percentages (0.0, 0.2, 0.4, 0.6, 0.8, 1.0, 3.0 and 5.0 wt%) by using solid-state method at 700 °C calcining temperature for 2 h. The resulted powders were ground in mortar for 30 min and subsequently pressed into disks at 12 tones for 10 min to obtain a 13-mm-diameter and ~ 0.7-mm-thick pellet. These pellets were sintered at 1100 °C for 6 h in air. The density of doped NBT samples was measured using densimeter (MD 300S) by the Archimedes principle. The average density of the samples is ~ 5.5 gcm^{-3}. The small amount of CeO_2 dopant (0.2–5.0 wt%) shows insignificant changes in the density value. Silver paste was applied on both surfaces of the disk and fired at 100 °C for 30 min to form a metal–insulator–metal (MIM) structure and used for electrical measurement.

The phase and crystal structure of NBT-*x* wt% CeO_2 were examined by X-ray diffractometer (Siemens D500). The particle size and morphology of NBT pellets were investigated by field emission scanning electron microscopy, FESEM (JEOL-JSM-7600F). The dielectric properties and piezoelectric resonance were measured using precision impedance analyzer (Agilent 4294A). The P-E hysteresis loop was measured using radiant technology precision LC analyzer. The sintered NBT ceramic pellets were poled at a temperature of 200 °C (near to the depolarization temperature T_d) then field-cooled to room temperature. The triangular temperature waveforms generated by LakeShore temperature controller with five different heating rates (0.6 $°Cs^{-1}$, 0.9 $°Cs^{-1}$, 1.2 $°Cs^{-1}$, 1.5 $°Cs^{-1}$ and 1.8 $°Cs^{-1}$) in the temperature range of 25 °C to 30 °C were applied to the samples. The resultant of short-circuited pyroelectric current was measured using Keithly 617 electrometer. Quasi-static method was used to measure the pyroelectric coefficient of the poled NBT samples.

3 Results

3.1 NBT samples at various weight percentages of CeO_2

NBT ceramics were doped with various weight percentages of CeO_2 from 0.2 to 5.0 wt%. The CeO_2-doped NBT samples change in color during the sintering process. The color of sintered ceramics has changed from light yellow to dark brown (vermilion) depending on the wt% of dopant. The color of the doped NBT becomes deeper gradually as the weight percentage of CeO_2 is increased (refer to Fig. 1). Similar results were reported for Ce-doped $(Na_{0.5}Bi_{0.5})_{0.93}Ba_{0.07}TiO_3$ [13] indicating the Ce ion has been incorporated into the NBT lattice and the volatilization of A-site element from NBT has caused oxidation during the sintering process [13, 14].

3.2 XRD analysis

Figure 2a shows the XRD pattern of CeO_2-doped NBT ceramics with different weight percentages (0.0–5.0 wt%). A single perovskite structure is observed when the weight percentage of CeO_2 is less than 1.0%. However, further increase of CeO_2 shows the characteristic peaks of the CeO_2. The CeO_2 was diffused into NBT lattice during the sintering process. However, when the amount of CeO_2 is above 1.0 wt%, CeO_2 tends to 'squeeze' out of the grain and accumulates at the grain boundary in the ceramics and becomes more conductive. Hence, 1.0 wt% was identified as the limit of CeO_2 as a dopant in the NBT ceramics.

Figure 2b shows the enlarged image of the XRD patterns in the range of 38°–48°. A splitting of the peaks was observed for the samples after the doping process. The pure NBT shows single rhombohedral perovskite structure. Doped samples exhibit tetragonal peaks which were observed from the split peaks (003/021) and (002/200), respectively [15]. The tetragonality of the ceramic lattice increased when the NBT ceramic was doped with higher percentage of CeO_2 [16]. The split peaks indicate rhombohedral–tetragonal morphotropic phase boundary in the NBT when doped with CeO_2 ceramic.

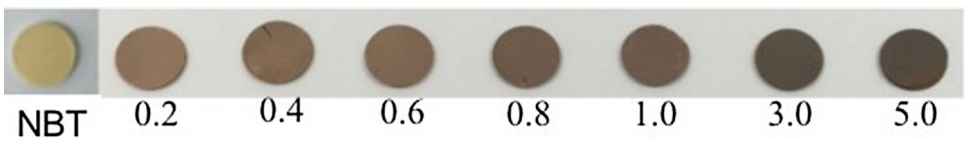

Fig. 1 NBT-*x* wt% CeO_2 pellets ($x = 0.0–5.0$)

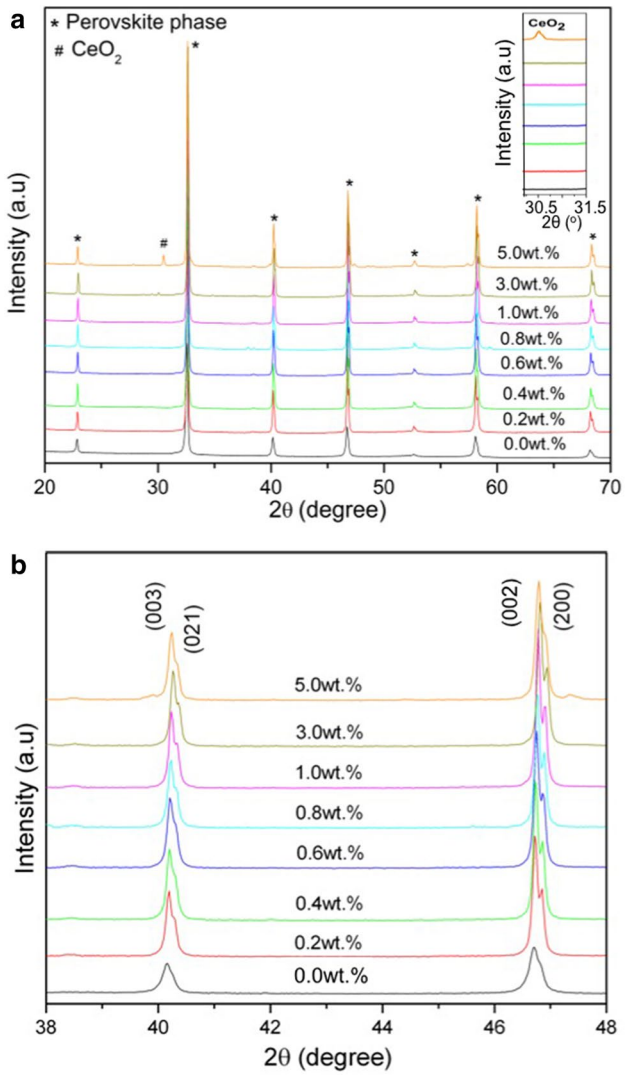

Fig. 2 X-ray diffraction pattern of NBT doped: **a** different amount of CeO_2 and **b** 2θ between 38° and 48°

3.2.1 Determination of crystallite size

The crystallite sizes of the CeO_2-doped NBT nanoparticles were determined by means of an X-ray line-broadening method using Scherrer equation [17]:

$$D = \frac{k\lambda}{\beta_{hkl}\cos\theta_{hkl}} \quad (1)$$

where D is the crystallite size in nanometers, λ is the wavelength of the radiation (1.54060 Å for CuKα radiation), k is the shape factor or the Scherrer constant ($k = 0.89$), β_{hkl} is the broadening of the hkl diffraction peak at half-maximum intensity in radians unit and θ_{hkl} is the Bragg diffraction angle, respectively. Two planes at 32.6° and 46.7°, which have the highest intensity, were selected for calculating the crystallite size. Table 1 shows the average of crystallite size of CeO_2-doped NBT nanoparticles calcined at 700 °C. The crystallite size of the NBT sample doped with 0.2% by weight CeO_2 is comparable to pure NBT, which is ~ 44 nm. However, the crystallite size was reduced from 44 ± 2 nm to 32 ± 2 nm as the weight percentage of CeO_2 increases to 0.6. Further increase in the weight percentage of CeO_2 (above 0.8 wt%) caused the crystallite size to increase to ~ 50 nm.

Table 1 The crystallite size of NBT-x wt% CeO_2

x wt% CeO_2	2θ(°) ± 0.1	FWHM ± 0.0001	Average crystallite size (nm) ± 2	
0.0	32.6	0.2263	43.8	44
	46.7	0.2863	44.5	
0.2	32.6	0.1661	43.3	43
	46.7	0.1158	43.0	
0.4	32.6	0.1685	35.3	35
	46.7	0.1067	35.0	
0.6	32.6	0.1675	31.5	32
	46.7	0.2063	31.8	
0.8	32.6	0.1624	49.0	48
	46.7	0.1037	48.6	
1.0	32.6	0.1570	50.7	50
	46.7	0.0983	50.3	
3.0	32.6	0.1559	51.0	51
	46.7	0.1048	50.7	
5.0	32.6	0.1601	49.7	50
	46.7	0.2115	50.2	

3.3 FESEM analysis

The micrographs of NBT-x wt% CeO_2 ceramics sintered at 1100 °C for 6 h are shown in Fig. 3. The micrograph shows that CeO_2 in the NBT caused a significant change in the grain size and the microstructure of the ceramic. Compared to that of pure NBT ceramic, the average grain size decreases from ~ 0.5 µm (pure NBT) to ~ 0.3 µm (0.6 wt%). The Ce ions restrain the grain growth during the sintering process. Moreover, the grains of the CeO_2-doped NBT are in square and rectangular shapes.

3.4 Dielectric properties

The temperature dependence of dielectric constant ε' and dissipation factor tan δ of NBT wt% CeO_2 at 10 kHz are shown in Fig. 4. Two characteristic temperatures: depolarization temperature T_d and temperature T_m at which maximum of electric permittivity exists were observed from the graph ε' versus T. T_d is a depolarization temperature at which long-range ferroelectric state starts to disturb. T_m is related to the dynamic effect due to the relaxation process, which

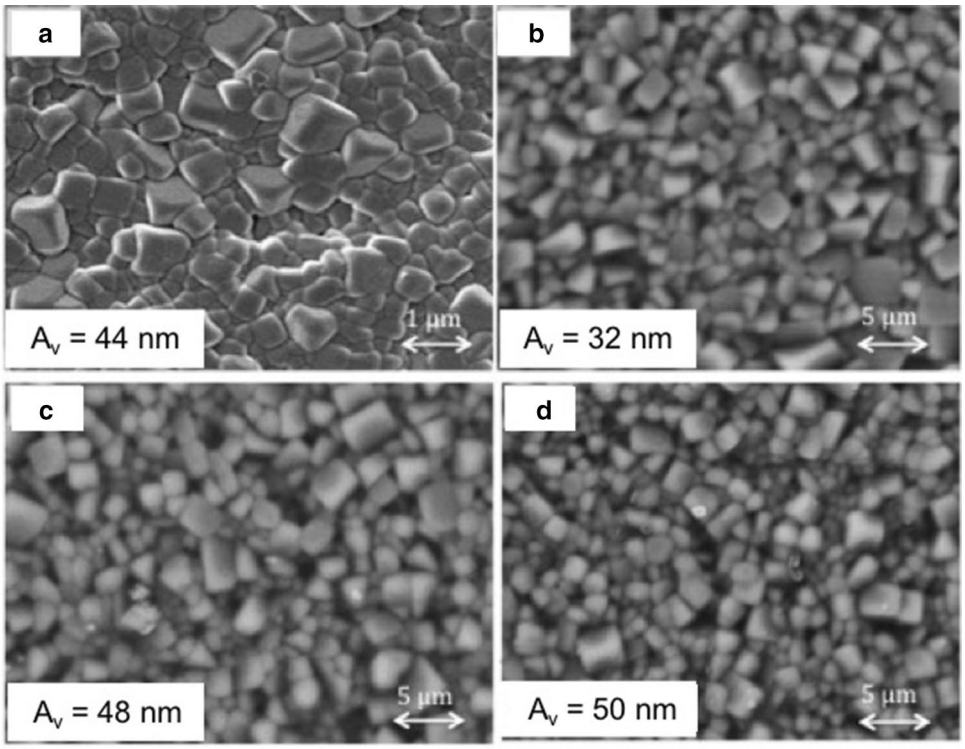

Fig. 3 The FESEM micrograph of NBT ceramics with CeO_2 additives **a** 0.0 wt%, **b** 0.6 wt%, **c** 0.8 wt% and **d** 1.0 wt%. The average size of the grain, A_v, ± 2 nm is given in the figure

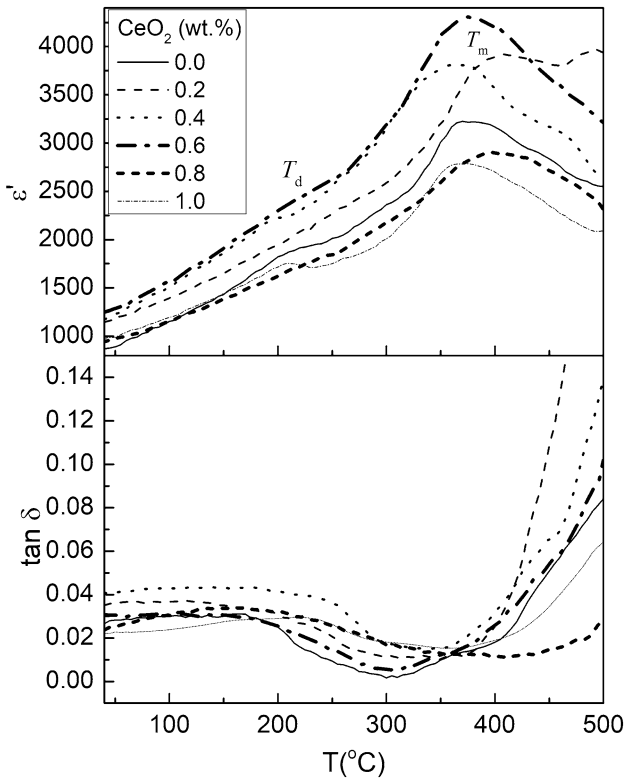

Fig. 4 Temperature dependence of dielectric constant ε′ and dissipation factor tan δ of CeO_2-doped NBT at 10 kHz

responds to the electromechanical interactions between polar regions and nonpolar matrix, but not corresponds to any phase transition [18, 19]. The T_d of the doped NBT samples is about 215 °C, while T_m shows some changes in the range of 350–370 °C.

The ε′ and tan δ increase with increasing of dopant weight percentage up to 0.6 wt%. Further increase in CeO_2 dopant wt% shows a decreasing trend in the ε′ and tan δ. It is attributed to the easy switching of the ferroelectric domain, which results in the increase of ε′ and tan δ. When the weight percentage of CeO_2 was above 0.8%, the excess CeO_2 stayed in the boundary and formed grain boundary layer that caused the reduction in ε′ [12].

3.5 Piezoelectric properties

The electromechanical coupling coefficient k is an indicator of the conversion efficiency between electrical and acoustic energy in a piezoelectric material. The aspect ratio of the piezoelectric resonance represents a bar poled along the long axis of the thickness direction, which yields electromechanical coupling coefficient k_{33}. The k_{33} is defined as [20]:

$$1 - k_{33}^2 = \frac{\varepsilon_{33}^S}{\varepsilon_{33}^T} \tag{2}$$

as described in [2] ε_{33}^T is the dielectric permittivity tensor under constant stress and ε_{33}^S is the dielectric permittivity

tensor under constant strain. The stiffness compliance constant (Young's modulus) c_{33} is an indicator of the stiffness or elasticity of a ceramic material. The Young's modulus can obtain from [20]:

$$f_t = \frac{1}{2t}\sqrt{\frac{C_{33}}{\rho}} \tag{3}$$

where t is the thickness of the ceramic, f_t is the resonance frequency and ρ is the density of the NBT ceramic. The piezoelectric constant d_{33} can be calculated from the equation below [20]:

$$d_{33} = k_{33}\sqrt{\varepsilon_0 \varepsilon_{33}^S s_{33}^D} \tag{4}$$

where s_{33} is the elastic constant, which is the reciprocal of the Young's modulus and ε_0 is the permittivity of free space (8.85×10^{-12} Fm^{-1}).

Figure 5 shows the thickness extensional (TE) resonance peak at room temperature for the ε' and tan δ. The intensity of tan δ or resonance peak increases by increasing of the CeO_2 dopant up to 0.6 wt% and then reduces after the doping percentage increases to 0.8 wt%. Meanwhile, the TE resonance frequency f_r (~ 3 MHz) has slightly shifted to the left and the intensity of the resonance peak decreases with the increasing of CeO_2 dopant, respectively.

The dielectric and piezoelectric properties of CeO_2-doped NBT are summarized in Fig. 6. The 0.6 wt% of CeO_2 shows the highest dielectric constant ε' of 1276, mechanical coupling factor k_{33} of 0.44 and piezoelectric

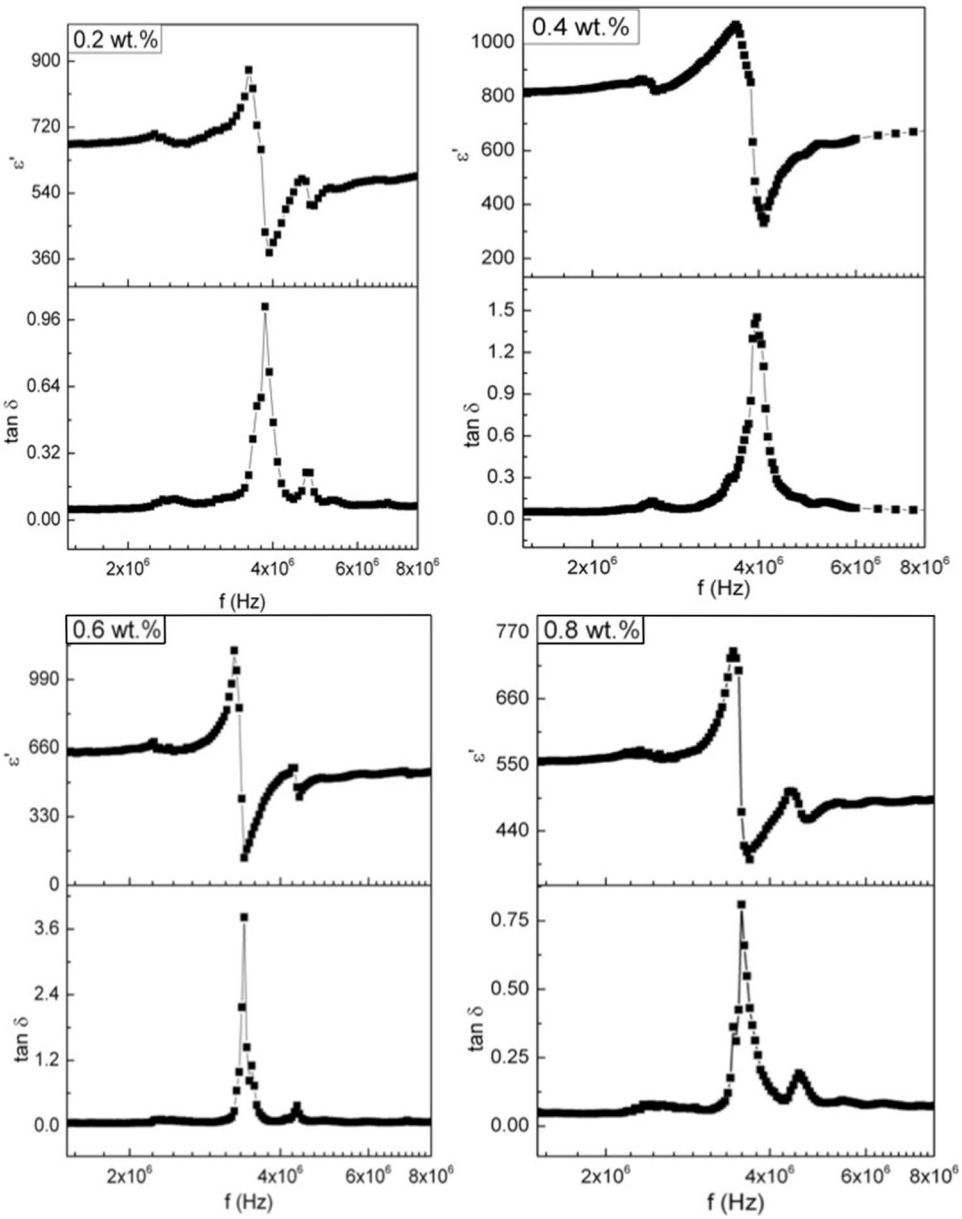

Fig. 5 Piezoelectric resonances at various weight percentages of CeO_2

constant d_{33} of 90 pC N^{-1}. The Young's modulus c_{33} decreases to 138 GPa. Excess doping of CeO_2 decreases the stiffness of the NBT piezoelectric constant. A soft dopant such as Ce ion may *soften* and increase the properties of piezoelectric ceramics; thus, dielectric constant ε' and electromechanical coupling factor k_{33} are enhanced, while it is also reported (see [21]) to reduce the coercive field E_c of the ceramic which will be discussed in the next section.

3.6 Ferroelectric properties

The polarization *P* versus electric field *E* (*P*-*E*) hysteresis loops of the NBT-*x* wt% CeO_2 ceramics at room temperature are shown in Fig. 7. At low applied voltage, the *P*–*E* curve is almost linear. When *E* increased, the hysteresis loops emerged rapidly where the dipoles in the NBT began to align gradually with the field and finally reached the saturation polarization. However, a fully saturated hysteresis loops were not obtained for these samples (see Fig. 7). This is probably due to the existence of oxygen vacancies and leakage current in the NBT ceramics.

Figure 8 shows the *P*–*E* hysteresis loops of the various CeO_2-doped NBT samples at a maximum applied electric field. The remanent polarization P_r of doped NBT is enhanced up to 0.6 wt%. Then the *P*–*E* loops become rounded and conductive as the CeO_2 weight percentages increase above 0.6 wt% due to the presence of excessive CeO_2. The coercive field E_c for CeO_2-doped NBT is reduced. The 0.6 wt % CeO_2-doped NBT exhibited the highest P_r of 56 μC cm^{-2} and has the lowest coercive field E_c of 53 kV cm^{-1}, respectively. The poling process causes a slight change in chargers in the B-site element of the perovskite structure. The charges caused charge defect, interact strongly with domain walls and consequently affect the ferroelectric behavior of the sample [22].

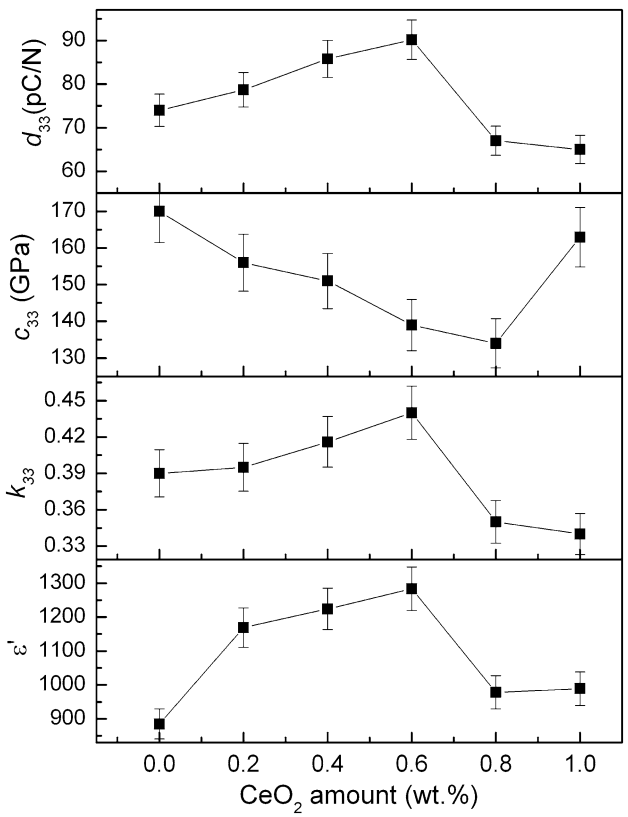

Fig. 6 Dielectric constant ε' and piezoelectric properties of CeO_2-doped NBT; piezoelectric constant d_{33}, Young's modulus c_{33} and mechanical coupling factor k_{33}

3.7 Pyroelectric properties

A triangular temperature waveform was applied to the samples (shown in Fig. 9a for NBT-0.6 wt% CeO_2), and a corresponding square waveform pyroelectric current was observed (refer to Fig. 9a). The resultant pyroelectric current is caused by the change in spontaneous polarization due to the temperature change. The accumulated surface charge density in the sample is allowed to flow when the temperature change can be defined as [23]:

$$I\mathrm{p} = p\mathrm{A}\frac{\mathrm{d}T}{\mathrm{d}t} \tag{5}$$

where I_p is the pyroelectric current, *p* is the pyroelectric coefficient, *A* is the electrode area and d*T*/d*t* is the heating rate.

The pyroelectric coefficients *p* of poled NBT samples are shown in Fig. 9b. The NBT-0.6 wt% CeO_2 shows the highest *p* (650 μC m^{-2} K^{-1}). Similarly, we observed the highest P_r for this sample (refer to Fig. 8). The *p* for the 0.2 wt% Ce-doped samples was lower than pure NBT. By referring to the temperature dependence of dielectric constant (see Fig. 4), the depolarization temperature of 0.2 wt% CeO_2 is above 200 °C compared to the rest of the compositions. However, the poling process of all the compounds was done at 200 °C to be consistent. Thus, the applied temperature during the poling process for 0.2 wt% CeO_2-doped NBT presumably not optimized for an effective poling. In addition, as the weight percentage of CeO_2 was increased to 1.0 wt%, the CeO_2-doped NBT ceramic became conductive and distorted the spontaneous polarization and consequently the pyroelectric coefficient decreased.

3.8 Leakage current

Figure 10 shows the leakage current density *J* versus electric field *E* curves of the CeO_2-doped NBT from 0.0 to 5.0 wt%. From the observation, it is obvious that high weight percentage of CeO_2 causes high leakage current and thus high conductivity. This is expected as CeO_2 is a

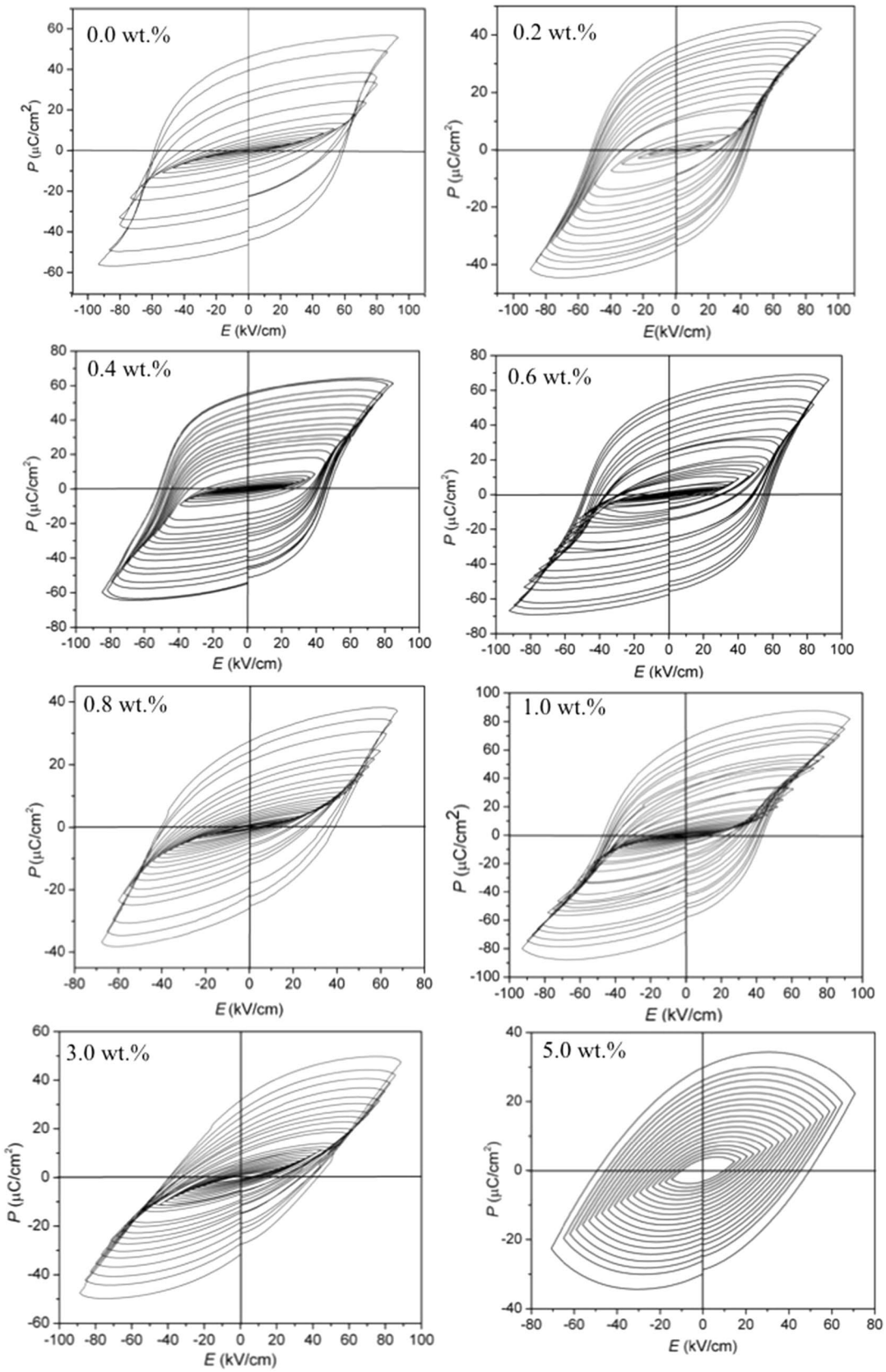

Fig. 7 *P–E* hysteresis loops of NBT-*x* wt% CeO_2 by increasing the step size of electric field

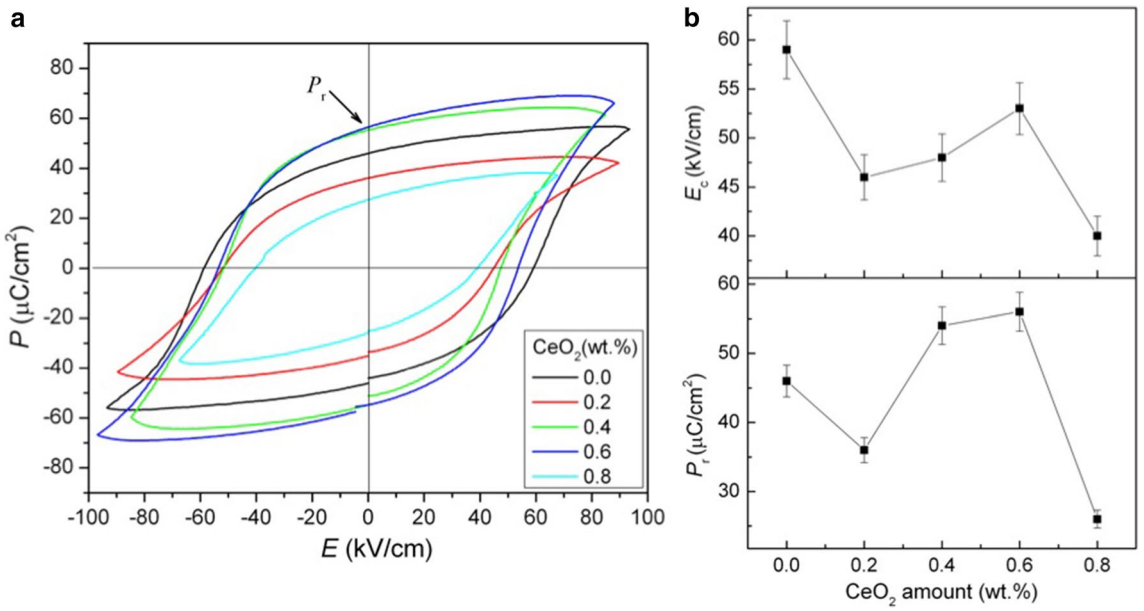

Fig. 8 **a** P–E hysteresis loops at various weight percentages of CeO_2 and **b** P_r and E_c of the NBT ceramics as a function of CeO_2

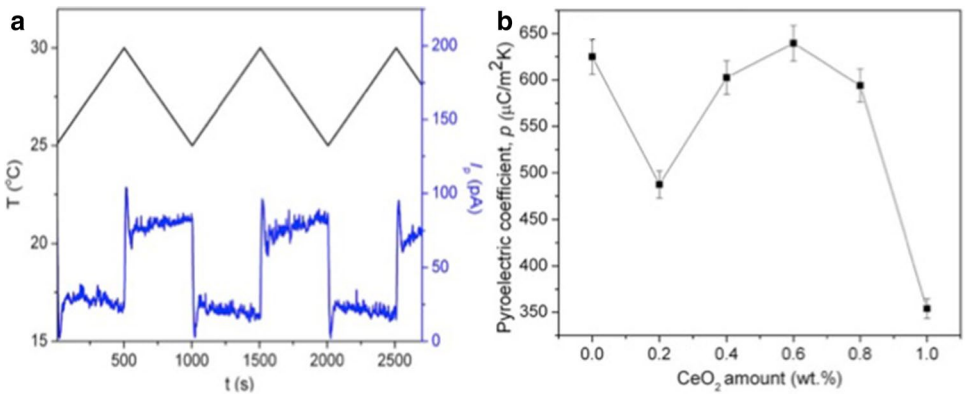

Fig. 9 **a** The pyroelectric current of poled NBT-0.6 wt% CeO_2 ceramic at the heating rate 0.6°Cs^{-1} and **b** pyroelectric coefficient of BNT ceramics

conductive material. However, a small amount of CeO_2 can significantly improve the electrical properties. The average of leakage current for the sample doped with 0.0 to 1.0 wt% of CeO_2 is about 10^{-6}–10^{-9} Acm^{-2} over the electric field range of ± 4 MV m^{-1}. The 0.6 wt% doped CeO_2 shows the lowest leakage current density (10^{-9} A cm^{-2}) and thus can be a good dielectric material.

4 Discussion

The results in the above sections show that doping CeO_2 in NBT improved the ferro-, pyro-, piezo- and dielectric properties of the ceramic. CeO_2 acts as both donor and acceptor in the NBT ceramic during the sintering process. Ce ion possibly exists in two valence states: Ce^{4+} (ionic radius of 0.97 Å) and Ce^{3+} (ionic radius of 1.01 Å). Since Ce ions are

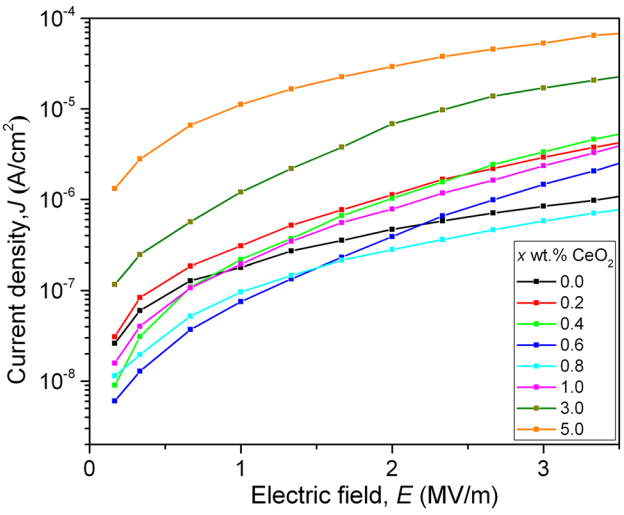

Fig. 10 Leakage current density of NBT-x wt% CeO_2 ceramics

larger, they are unable to reside in B-site of the NBT perovskite where originally only resided by Ti^{4+} (ionic radius of 0.605 Å). However, Ce ions can occupy the A-site of the ceramic, including A1-site (Na^{+} in ionic radius of 0.99 Å) and A2-site (Bi^{3+} in ionic radius of 0.96 Å) [24]. Logically, either Ce^{3+} or Ce^{4+} occupies Bi^{3+}-site in the NBT. It is known that Bi_2O_3 is volatile at high temperature during the sintering process and Bi^{3+} in the NBT causes some vacancies of A-site in the lattice. The replacement of A-site by Ce^{3+} or Ce^{4+} does not cause any deformation in the NBT lattice, as there is no evident that the domain movement has been enhanced. However, Ce^{4+} ion has smaller radius and also has the same charge as that of Ti ion and may occupy the B-site. The doping of Ce^{4+} into Ti^{4+}-site in the NBT ceramics increases the space charges (i.e., both charges and hole carries). These space charges cause an internal field inside the grains of NBT, and this field may inhibit the domain movement of the domain walls. The dislocation of Ce^{4+} atoms may cause a defect in the lattice during the poling process and thus result in higher piezoelectric and ferroelectric properties [25].

When the amount of CeO_2 is over 0.8 wt%, some of the Ti^{4+} ions may be substituted by Ce^{4+} in the lattice of the NBT ceramic. In addition, excess Ce ions may accumulate in the grain boundaries causing the pinning effect on the domains which consequently hinder their motion and reduced the stability of the ferroelectric domains. This results the deterioration of piezo- , pyro- and ferroelectric properties of the samples.

The structure with a composition at the morphotropic phase boundary (MPB) is considered as a transitional phase structure between tetragonal and the rhombohedral phases. The lattice structure may change by an external field, and the evolution in the crystal structure from the rhombohedral phase to morphotropic phase boundary shows a positive effect on the electrical properties. At the morphotropic phase boundary, the materials can be both rhombohedral and tetragonal phase, and spontaneous polarization can be moved along any one of the 14 directions. Consequently, it is easier for the domain to move during the poling process which results in the higher piezoelectric and dielectric properties [26].

5 Conclusions

The dielectric, piezoelectric, pyroelectric and ferroelectric properties of CeO_2-doped NBT at various weight percentages have been investigated. The pure NBT exhibits the perovskite structure in the rhombohedral phase, while doping of CeO_2 has changed the structure into pure perovskite with morphotropic phase boundary of rhombohedral and tetragonal phase. The grain size of the ceramics slightly decreases after doping process. The 0.6 wt% of CeO_2-doped NBT ceramic is the optimized dopant concentration, where the NBT shows the highest piezoelectric constant d_{33} of 90 pC N^{-1}, electromechanical coupling coefficient k_{33} of 0.44, Young's modulus c_{33} of 138 GPa, remanent polarization P_r of 56 μC cm^{-2} and pyroelectric coefficient p of 650 μC m^{-2} K^{-1}, respectively.

Acknowledgements This work was supported by University of Malaya under the PPP Grant PG010-2013B and UMRG Grant RP038D-17AFR.

Compliance with ethical standards

Conflict of interest On behalf of all authors, the corresponding author states that there is no conflict of interest.

References

1. Gomah-Pettry J-R, Marchet P, Mercurio J-P (2004) Sodium–bismuth titanate based lead-free ferroelectric materials. J Eur Ceram Soc 24:1165–1169
2. Halim NA, Velayutham TS, Majid WHA (2016) Pyroelectric, ferroelectric, piezoelectric and dielectric properties of $Na_{0.5}Bi_{0.5}TiO_3$ ceramic prepared by sol-gel method. Ceram Int 42:15664–15670
3. Chu B-J, Chen D-R, Li G-R, Yin Q-R (2002) Electrical properties of $Na_{0.5}Bi_{0.5}TiO_3$–$BaTiO_3$ ceramics. J Eur Ceram Soc 22:2115–2121
4. Li H-D, Yao W-L (2004) Some effects of different additives on dielectric and piezoelectric properties of $(Bi_{0.5}Na_{0.5})TiO_3$–$BaTiO_3$ morphotropic-phase-boundary composition. Mater Lett 58:1194–1198
5. Fu P, Xu Z, Chu R, Li W, Zang G, Hao J (2010) Piezoelectric, ferroelectric and dielectric properties of La_2O_3-doped $(Bi_{0.5}Na_{0.5})_{0.94}Ba_{0.06}TiO_3$ lead-free ceramics. Mater Des 31:796–801
6. Fu P, Xu Z, Chu R, Li W, Zang G, Hao J (2010) Piezoelectric, ferroelectric and dielectric properties of Nd_2O_3-doped $(Bi_{0.5}Na_{0.5})_{0.94}Ba_{0.06}TiO_3$ lead-free ceramics. Mater Sci Eng B 167:161–166
7. Shi J, Yang W (2009) Piezoelectric and dielectric properties of CeO_2-doped $(Bi_{0.5}Na_{0.5})_{0.94}Ba_{0.06}TiO_3$ lead-free ceramics. J Alloy Compd 472:267–270
8. Wang X, Chan HL-W, Choy C-L (2003) Piezoelectric and dielectric properties of CeO_2-added $(Bi_{0.5}Na_{0.5})_{0.94}Ba_{0.06}TiO_3$ lead-free ceramics. Solid State Commun 125:395–399
9. Zhou C, Liu X, Li W, Yuan C (2009) Dielectric and piezoelectric properties of Y_2O_3 doped $(Bi_{0.5}Na_{0.5})_{0.94}Ba_{0.06}TiO_3$ lead-free piezoelectric ceramics. Mater Res Bull 44:724–727
10. Garg A, Agrawal DC (1999) Structural and electrical studies of CeO_2 modified lead zirconate titanate ceramics. J Mater Sci Mater Electron 10:649–652
11. Shan D, Qu Y, Song J (2007) Ionic doping effects on crystal structure and relaxation character in $Bi_{0.5}Na_{0.5}TiO_3$ ferroelectric ceramics. J Mater Res 22:730–734
12. Zhang R, Yang Z, Chao X, Kang C (2009) Effects of CeO_2 addition on the piezoelectric properties of PNW–PMN–PZT ceramics. Ceram Int 35:199–204
13. Chen M, Xu Q, Kim BH, Ahn BK, Chen W (2008) Effect of CeO_2 addition on structure and electrical properties of $(Na_{0.5}Bi_{0.5})_{0.93}Ba_{0.07}TiO_3$ ceramics prepared by citric method. Mater Res Bull 43:1420–1430
14. Awang Rozidawati, Ab Nurain, Halim Zalita Zainuddin, Jumali Mohammad Hafizuddin Haji, Yahya Muhammad, Salleh Muhammad Mat (2012) Fundamental study on microstructure of

CeO_2-doped $(Na_{0.5}Bi_{0.5})TiO_3$ ceramics. Solid State Sci Technol 20:109–114
15. Guo Huiling, Li Yang, Zhang Yong, Sun Huajun, Liu Xiaofang (2018) Improved electrical properties of Co-doped 0.92NBT-0.04KBT-0.04BT lead-free ceramics. J Mater Sci Mater Electron 29:19063–19069
16. Liao Y, Xiao D, Lin D, Zhu J, Yu P, Wu L, Wang X (2006) The effects of CeO_2-doping on piezoelectric and dielectric properties of $Bi_{0.5}(Na_{1-x-y}K_xLi_y)_{0.5}TiO_3$ piezoelectric ceramics. Mater Sci Eng B 133:172–176
17. Panigrahi MR, Panigrahi S (2010) Structural analysis of 100% relative intense peak of $Ba_{1-x}Ca_xTiO_3$ ceramics by X-ray powder diffraction method. Physica B 405(7):1787–1791
18. Suchanicz J, Mercurio JP, Konieczny K (2002) Electric properties of $(Na_{0.5}Bi_{0.5})_{0.86}Ba_{0.14}TiO_3$ single crystal. Ferroelectrics 268:357–362
19. Suchanicz J, Kluczewska K, Czaja P, Kania A, Konieczny K, Handke B, Sokolowski M, Trubitsyn MP, Kruzina TV (2017) The influence of electric poling on structural, thermal, dielectric and ferroelectric properties of $Na_{0.5}Bi_{0.5}TiO_3$ ceramics. Ceram Int 43:17194–17201
20. Jaffe B (2012) Piezoelectric ceramics, vol 3. Elsevier, Amsterdam
21. Xu Y (1991) Ferroelectric Materials and Their Applications. North-Holland, The Netherlands
22. Kontsos A, Landis CM (2009) Computational modeling of domain wall interactions with dislocations in ferroelectric crystals. Int J Solids Struct 46:1491–1498
23. Furukawa T, Wen JX, Suzuki K, Takashina Y, Date M (1984) Piezoelectricity and pyroelectricity in vinylidene flouride/trifloroethylane copolymers. J Appl Phys 56:829
24. Shannon RD (1976) Revised effective ionic radii & systematic studies of interatomic distances in Halides & Chalcogenides. Acta Cryst. A32:751–767
25. Li Y, Chen W, Xu Q, Zhou J, Wang Y, Sun H (2007) Piezoelectric and dielectric properties of CeO_2-doped $Bi_{0.5}Na_{0.44}K_{0.06}TiO_3$ lead-free ceramics. Ceram Int 33:95–99
26. Zhao S, Wu H, Sun Q (2005) Study on PSN–PZN–PZT quaternary piezoelectric ceramics near the morphotropic phase boundary. Mater Sci Eng B 123:203–210